Available online at www.sciencedirect.com
SCIENCE DIRECT®
Journal of Nuclear Materials 342 (2005) 90–100
journal of nuclear materials
www.elsevier.com/locate/jnucmat

Swelling and radiation-induced segregation in austentic alloys

T.R. Allen [a,*], J.I. Cole [b], J. Gan [b], G.S. Was [c], R. Dropek [c], E.A. Kenik [d]

[a] University of Wisconsin, 1500 Engineering Drive, Madison, WI 53706, USA
[b] Argonne National Laboratory-West, USA
[c] University of Michigan, USA
[d] Oak Ridge National Laboratory, USA

Received 4 October 2004; accepted 16 February 2005

Abstract

To elucidate the relationship between radiation-induced segregation and swelling in austenitic stainless steels, a series of alloys were irradiated with 3.2 MeV protons to doses of 0.5 and 1.0 dpa at 400 °C. Three alloy series were irradiated, the first to examine the effect of bulk nickel in Fe–16–18Cr–*x*Ni, the second to determine the effect of Mo and P in an Fe–16Cr–13Ni base alloy, and the third to examine the effect of oversized solute Zr addition to an Fe–18Cr–0.5Ni alloy. The addition of nickel in Fe–16–18Cr–*x*Ni caused a significant decrease in swelling and increase in segregation. The addition of Mo+P to Fe–16Cr–13Ni eliminated swelling and reduced segregation. The addition of Zr to Fe–18Cr–9.5Ni decreased swelling and altered the segregation. Comparison of swelling with changes in lattice parameter and shear modulus caused by the segregation showed that swelling correlates well with the decreases in lattice parameter caused by radiation-induced segregation. Those alloys whose segregation decreased the lattice parameter the greatest showed the lowest swelling. These results are consistent with theoretical predictions made by Wolfer.

1. Introduction

Void swelling in austenitic alloys can cause unacceptable dimensional changes in reactor structural materials. After void swelling was discovered in irradiated austenitic stainless steels [1], many studies were undertaken to determine not only the magnitude of the swelling problem but also the variables that influenced swelling. A comprehensive review of void swelling data is contained in reference [2].

The composition of austenitic steels strongly affects swelling. Fig. 1 shows the swelling as a function of bulk nickel composition for alloys with 16–18 wt% Cr [3–5]. Regardless of irradiation source (neutrons, heavy ions, or protons), the swelling decreases rapidly with increasing bulk nickel concentration.

Minor elements also affect swelling. Additions of P cause an increase in swelling with a peak swelling corresponding to an addition of ~0.02 wt% P [2]. As the P concentration is increased above ~0.02 wt% the swelling at temperatures decreases rapidly, This non-monotonic effect of P on swelling has been seen at temperatures from 400 to 540 °C. For temperatures between 400 and 600 °C, small amounts of Mo (0.5–1.0 wt%) caused swelling to increase in Fe–18Cr–8Ni alloys, but larger amounts caused swelling to decrease [2]. For 316 base materials irradiated at 500 °C with 1 MeV electrons, Kato et al. [6], found that the addition of Zr caused the void swelling to decrease dramatically. For the same

* Corresponding author. Tel.: +1 608 265 4083.
E-mail address: allen@engr.wisc.edu (T.R. Allen).

0022-3115/$ - see front matter © 2005 Elsevier B.V. All rights reserved.
doi:10.1016/j.jnucmat.2005.02.008

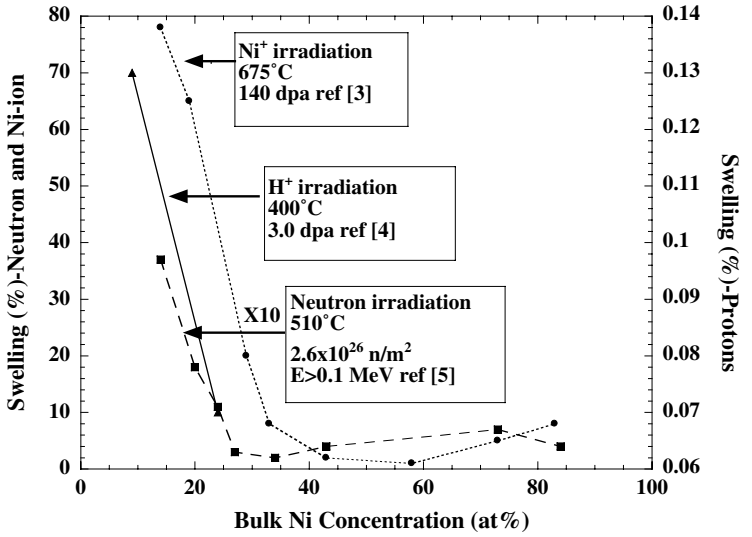

Fig. 1. The effect of bulk nickel concentration on swelling. Ni^+ ion irradiation data from [3]. Proton irradiation data from [4]. Neutron irradiation data from [5].

irradiation conditions, Kato et al. [7] showed that the addition of Zr decreased the grain boundary Cr depletion and nickel enrichment. Kato proposed that oversized elements added to the matrix act as recombination centers for point defects, decreasing radiation-induced processes like swelling and radiation-induced segregation (RIS).

In a series of recent studies, Garner has shown that at temperatures near 300–400 °C, the swelling in austenitic stainless steels increases if the radiation occurs at a lower displacement rate [8–14]. The increased swelling occurs due to a shortening of the transient region of swelling with materials exposed at lower displacement rates reaching the terminal swelling rate of 1%/dpa sooner.

All of these changes in swelling behavior are linked to key microstructural changes. In an experiment performed at ORNL, increasing the bulk nickel content from Fe–15Cr–15Ni to Fe–15Cr–35Ni was shown to decrease swelling by increasing the critical void radius above which void growth was energetically favorable [15]. The increase in critical radius corresponded with a change in dislocation microstructure, with higher nickel concentration leading to a larger concentration of faulted loops, which are weaker sinks for vacancies than dislocation networks. Okita and Wolfer [16], examining an Fe–15Cr–16Ni ternary alloy irradiated in FFTF, recently showed that the displacement rate dependence of void swelling occurs due to changes in the void density rather than the void size. The dislocation density also increased at lower displacement rate, changing in a manner similar to the void density. In both the ORNL work and the recent Okita study, the swelling development was consistent with the classic argument that the relative bias for point defects between dislocation loops and voids was responsible for the swelling behavior.

Radiation-induced segregation is a non-equilibrium process that occurs at grain boundaries and other defect sinks such as dislocation loops and voids during irradiation of an alloy at high temperature (30 to 50 percent of the melting temperature) [17]. In irradiated iron–chromium–nickel alloys, nickel enriches and chromium depletes at defect sinks. Iron either enriches or depletes depending on the bulk alloy composition. Marwick noted that accumulation of the slow-diffusing nickel to void surfaces in iron–chromium–nickel alloys could reduce the rate of void growth by reducing the arrival rate of vacancies to the void surface [18]. Marwick postulated that differences in diffusion rates between different iron–chromium–nickel alloys might explain the differences in swelling behavior.

Wolfer et al. have also theoretically predicted that segregation will change the bias of defect sinks for point defects [19–21]. Because a difference in bias for point defects between dislocations and cavities is required for swelling to occur, segregation may alter the net bias and thus alter the swelling. Since measurements have shown that swelling in austenitic stainless steels ultimately reaches a terminal rate of 1%/dpa, any effect of segregation on swelling during void growth is likely to occur during the transient phase of void swelling, consistent with the work of Okita [16].

Detailed studies of RIS in iron–chromium–nickel alloys have recently been completed which allow a more complete understanding of the effect of microstructural changes on swelling. This paper reports on a series of

swelling and segregation measurements and places that data in the context of the previous theoretical studies on changing the net bias for point defect absorption.

2. Experiment

Eight separate alloys were tested in this work, Table 1. The alloys are grouped into three sets, each set supporting a separate investigation, the effect of bulk nickel, the effect of minor element additions Mo and P, and the effect of adding an oversized element, specifically zirconium. The effect of bulk nickel, the effect of the addition of minor elements Mo and P, and the addition of the oversized solute Zr were chosen with the expectation that they would affect swelling and segregation through different mechanisms. The bulk nickel series was chosen to assess bulk diffusivity effects, the Mo and P to look at chemical ordering effects, and the zirconium series to address the effect of oversized solutes. The three elements of the test matrix are presented in Table 2.

General Electric Global Research in Schenectady, NY produced all the alloys used in this project. The as-received materials were solution annealed at 1200 °C for one hour and quenched in water. Each alloy was cold-worked to a 66% thickness reduction by cold rolling. Samples of TEM coupons were then fabricated using electrical discharge machining (EDM). Samples underwent a recrystallization anneal to obtain an average grain size of around 20 μm. Twenty-micrometer grains were desired because the range of damage of 3.2 MeV protons used to irradiate samples is approximately 40 μm. An irradiation depth of 40 μm ensures that, on average, multiple complete grains are irradiated prior to testing for crack initiation.

Sample irradiations were performed using the General Ionex Tandetron accelerator in the Michigan Ion Beam Laboratory at the University of Michigan. Irradiations were conducted using 3.2 MeV protons at a dose rate of approximately 8×10^{-6} dpa/s. The samples were irradiated at 400 °C to a final dose of 0.5 or 1 dpa. Details of the sample irradiation procedure can be found in Ref. [21].

Table 2
Test matrix

Alloys
Bulk nickel series
Fe–18Cr–8Ni–1.25Mn
Fe–16Cr–13Ni–1.25Mn
Fe–18Cr–40Ni–1.25Mn
316 series
Fe–16Cr–13Ni–1.25Mn
Fe–16Cr–13Ni–1.25Mn+Mo
Fe–16Cr–13Ni–1.25Mn+Mo+P
Zirconium series
Fe–18Cr–9.5Ni–1.75Mn
Fe–18Cr–9.5Ni–1.75Mn+0.04Zr
Fe–18Cr–9.5Ni–1.75Mn+0.16Zr

Void and dislocation loop distributions were measured using a JEOL 2010 TEM. Analysis was carried out in the TEM operating at an accelerating voltage of 200 kV. Sample thickness for cavity density measurements was determined using convergent beam electron diffraction (CBED) at $g = 311$. The density and size of voids were measured from bright-field images with electron beam condition away from any strong diffraction conditions. The density and size of Frank loops were measured from the rel-rod dark-field images in which only faulted loops are present [22,23]. Each TEM sample was examined to determine if there were any precipitates before and after irradiation. Swelling is determined from the void size distribution measured using transmission electron microscopy.

Grain boundary compositions were measured using scanning transmission electron microscopy with energy dispersive X-ray spectrometry (STEM/EDS). The STEM/EDS was performed at an accelerating voltage of 200 kV on a Philips CM200 equipped with a field emission gun source at Oak Ridge National Laboratory. STEM/EDS measurements were performed at the grain boundary and at increments of 1.0 nm away from the boundary to give compositional profiles. The incident probe thickness was approximately 1.4 nm (full width, tenth maximum). The sample was tilted towards the X-ray detector and each grain boundary analyzed was

Table 1
Alloy composition (wt%)

Alloy designation	Fe	Cr	Ni	Mn	Mo	P	Zr	C
Fe–18Cr–8Ni–1.25Mn	72.4	18.1	8.4	1.1	<0.01	<0.01	<0.01	0.01
Fe–18Cr–9.5Ni–1.75Mn	70.0	18.6	9.7	1.74	<0.01	<0.01	<0.01	<0.01
Fe–16Cr–13Ni–1.25Mn	70.3	15.6	12.9	1.2	<0.01	<0.01	<0.01	0.01
Fe–18Cr–40 Ni–1.25Mn	40.0	18.1	40.7	1.2	<0.01	<0.01	<0.01	0.01
Fe–16Cr–13Ni–1.25Mn+Mo	68.4	15.4	13.2	1.2	1.85	<0.01	<0.01	0.01
Fe–16Cr–13Ni–1.25Mn+Mo+P	68.5	15.4	13.0	1.2	1.83	0.05	<0.01	0.01
Fe–18Cr–9.5Ni–1.75Mn–0.04Zr	69.1	19.1	10.0	1.74	<0.01	<0.01	0.04	0.02
Fe–18Cr–9.5Ni–1.75Mn–0.16Zr	70.3	18.2	9.6	1.75	<0.01	<0.01	0.16	<0.01

aligned such that the boundary was 'edge-on' (parallel to the electron beam). This alignment minimizes the effect of geometric broadening of the measured profiles by an inclined boundary.

3. Results

The swelling and segregation measurements for the Fe–(16–18)Cr–xNi (x = 8, 18, 40) alloys are plotted in Fig. 2. Uncertainty bars for the swelling are calculated from the uncertainty in the void density and size measurements. Uncertainty bars for the segregation are the standard deviation of the mean for the series of measurements. Consistent with previous studies, the swelling decreases with increasing bulk nickel. The enrichment of nickel and depletion of chromium also increase with increasing bulk nickel concentration. The loop and void size and density are plotted in Fig. 3. Consistent with the work of Okita on the effect of displacement rate [16], the effect of bulk nickel on swelling occurs in the void density and not the void size.

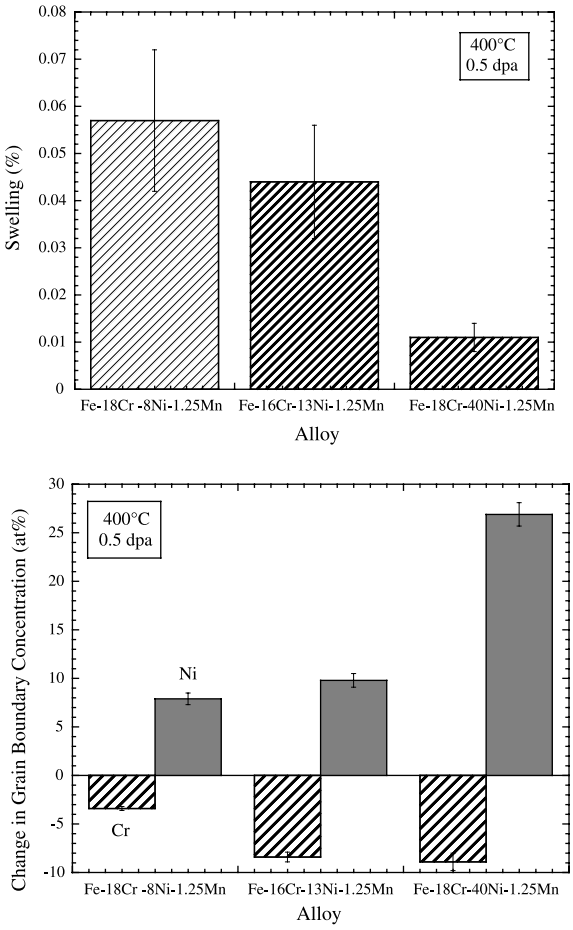

Fig. 2. Swelling and radiation-induced segregation as a function of composition for Fe–(16–18)Cr–X Ni with X = 8, 18, 40.

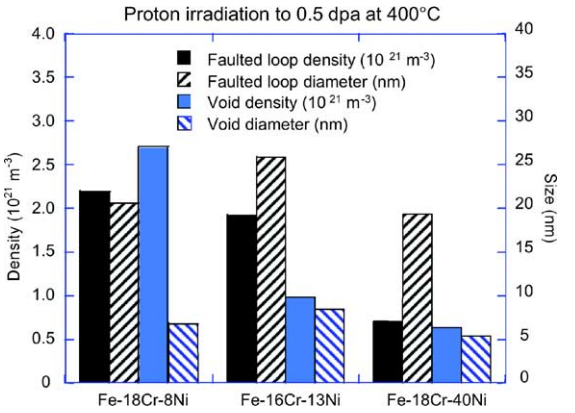

Fig. 3. Void and loop density and size as a function of bulk nickel concentration.

Fig. 4 shows the swelling and grain boundary segregation measurements for the Fe–16Cr–13Ni (+Mo, +Mo+P) alloys. The addition of molybdenum increased the swelling at 0.5 dpa while the addition of molybdenum and phosphorus significantly decreased the swelling. Although not shown, the swelling change corresponds to a change in void density and not size. In other studies [2], the effect of phosphorus on suppressing voids in neutron-irradiated stainless steels is typically explained by needle-shaped phosphorus precipitates, where clustering of Mo and P has been found. No phosphorus precipitates were observed in this study. The addition of molybdenum caused an increase in nickel enrichment and a decrease in chromium depletion at grain boundaries. The addition of molybdenum and phosphorous caused a decrease in nickel enrichment and chromium depletion at grain boundaries.

Fig. 5 shows the swelling and grain boundary segregation measurements for the Fe–18Cr–9.5Ni (+Zr) alloys. The addition of Zr decreased the swelling. Although not shown, the swelling change as zirconium is added corresponds to a change in void density and not size. The addition of zirconium caused a decrease in nickel enrichment but an increase in chromium depletion at grain boundaries. The Fe segregation is not shown in Fig. 5, but the addition of Zr caused Fe to switch from a depleting species to an enriching species. The addition of zirconium has changed the relative diffusivities such that iron is slower than average in the Zr-containing alloys. The Zr may preferentially interact with iron. Because the zirconium-containing alloys were irradiated to higher dose than the base alloy, the greater chromium depletion could be either a function of composition or dose. These experiments did not resolve the effect.

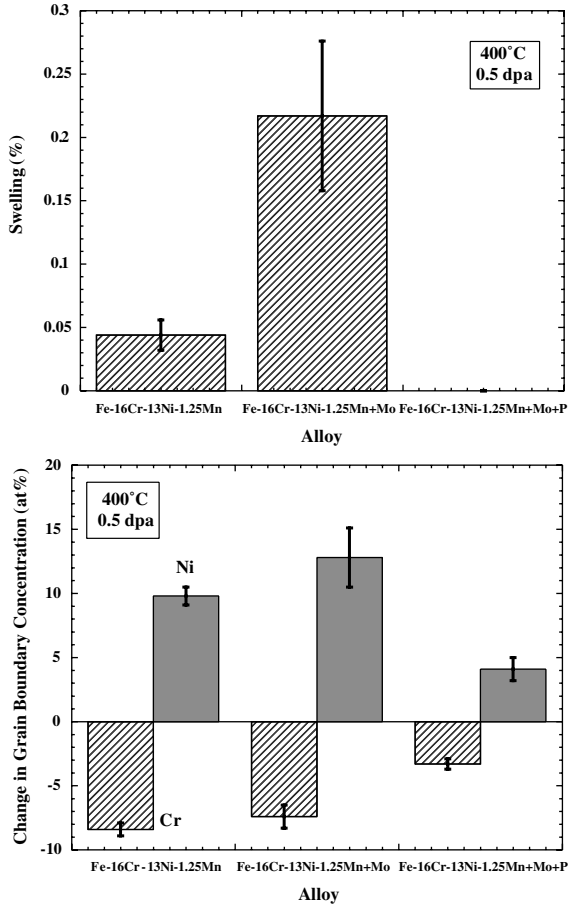

Fig. 4. Swelling and radiation-induced segregation as a function of composition for Fe–16Cr–13Ni (+Mo, +Mo+P).

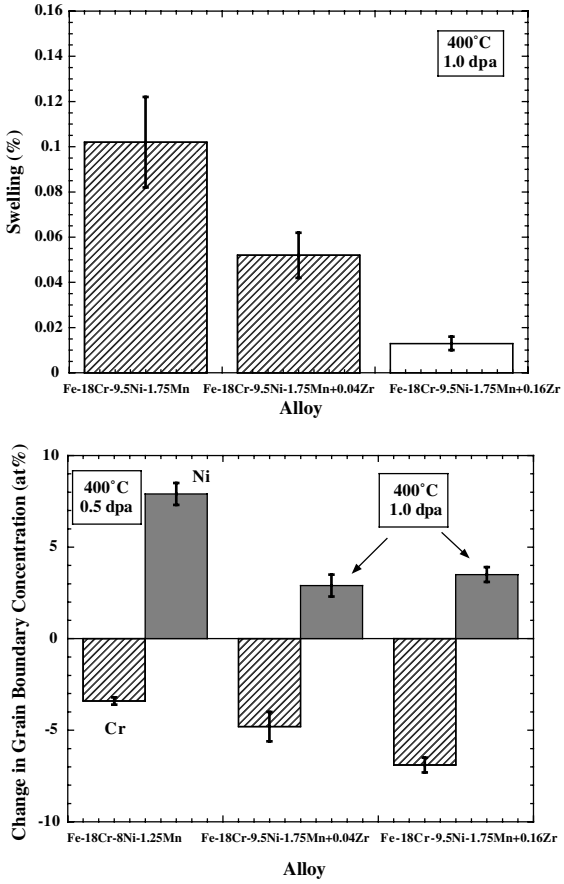

Fig. 5. Swelling and radiation-induced segregation as a function of composition for Fe–18Cr–9.5Ni (+Zr). The 'base alloy' for this graph is from the Ni-series, which has a slightly different base composition and was irradiated to only half the dose.

RIS in austenitic Fe–Cr–Ni alloys is primarily driven by interaction with the vacancy flux [30]. Atoms that diffuse faster than average in the alloy will deplete at boundaries while slower atoms will enrich. The changing segregation with the addition of minor elements is likely to be caused by changes in diffusivity relative to the average diffusivity in the alloy. In the Zr-series, chromium depletion increased while nickel enrichment decreased with the addition of Zr, indicating an increase in the diffusivity of chromium (relative to the alloy average) and a decrease in the diffusivity of nickel (relative to the alloy average). Segregation in the 316 + Mo + P alloy decreases relative to the base alloy. Therefore, the addition of Mo and P must alter the relative diffusion rates of iron, chromium, and nickel to reduce the segregation. Both chromium and phosphorous, and molybdenum and phosphorous are known to have attractive potentials [32]. The addition of phosphorus, which enriches at the boundary, may act as a pin for chromium and molybdenum, thus reducing the depletion. Previous work by Damcott et al. [33] showed that the addition of P to an Fe-18Cr–8Ni alloy increased both the chromium enrichment and nickel depletion. Therefore, adding P alone appears to increase segregation while the addition of Mo and P decrease the segregation. The attractive force is greater between Mo and P than between Cr and P. Apparently, the presence of Mo is critical to decreasing the overall segregation.

4. Discussion

As shown in previous works [15,19–21], the development of voids is dependent on the relative bias for point defects between dislocations and cavities, and that microchemical changes at cavity surfaces and dislocation cores can affect the point defect bias. In this section, the relationship between RIS and void development will be explored. Radiation-induced segregation occurs at grain boundaries, voids, and dislocation loops. As voids

and loops are surrounded by bulk material, the measurement of RIS is easier and more accurate at grain boundaries than at voids or loops. RIS profiles show similar trends at void surfaces as they do at grain boundaries [25]. This similarity in grain boundary and void RIS is used in the discussion below to elucidate the affect of RIS on swelling. Measured grain boundary segregation profiles will be used as surrogates for segregation profiles at void surfaces in estimating the effect of segregation on void swelling.

4.1. Correlations between swelling and RIS

In examining the effect of bulk nickel concentration on swelling, an interesting correlation between RIS and swelling is evident. Fig. 6 shows the ratio of chromium depletion to nickel enrichment for alloys with similar bulk chromium concentrations, but differing bulk nickel concentrations. The trends in this ratio of segregation are very similar to those of swelling (Fig. 1). For alloys with a small chromium-to-nickel depletion ratio (large nickel enrichment compared to chromium depletion), swelling is smaller. A relationship between swelling and RIS is suggested by the data.

Fig. 7 shows that the development of the segregation as a function of dose at 400 °C is quite different for varying alloy compositions. Those alloys with lower bulk nickel concentration develop RIS at a slower rate. Since the alloys with lower bulk nickel are also the higher swelling alloys, this data also suggests a possible origin for the relationship between swelling and RIS. Based on this observation, previous work described how RIS can decrease the overall vacancy flux to a void by increasing the strength of thermal back diffusion of the segregated atoms [34].

As noted in the introduction, recent work by Garner has shown that, in 304 stainless steel irradiated near 400

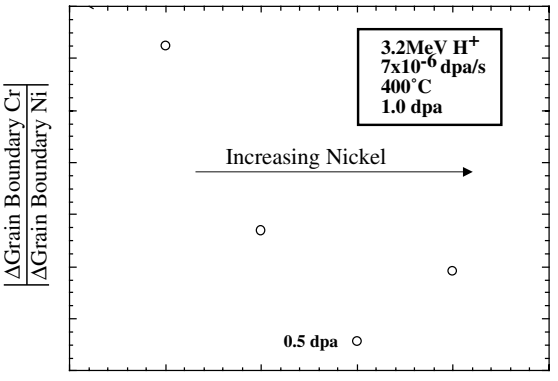

Fig. 6. Ratio of the change in grain boundary chromium depletion to nickel enrichment as a function of bulk nickel concentration. Data for Fe–20Cr–9Ni, Fe–20Cr–24Ni, and Ni–18Cr–9Fe from [26]. Data for Fe–18Cr–40Ni from this work.

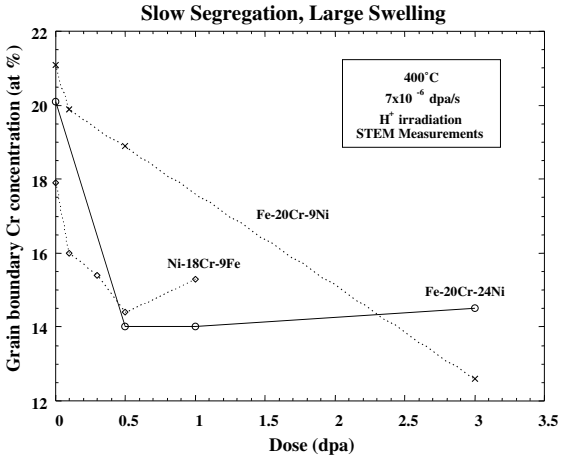

Fig. 7. Segregation as a function of dose for alloys with similar bulk chromium concentration but varying bulk nickel concentration. Data from [26,27].

°C, swelling is greater at lower displacement rates [8]. The data for Garner's study came from hex cans irradiated in the EBR-II reactor. Calculations indicate that for decreasing dose rate, the grain boundary segregation reaches steady-state more rapidly (in dose) [28]. RIS measurements on samples taken from the same EBR-II hex cans used in the Garner study show that the chromium depletion and nickel enrichment is greater at lower displacement rates [29]. In a similar manner as the data shown in Fig. 6, the chromium depletion to nickel enrichment ratio was the smallest for those alloys that showed the least swelling.

For swelling both as a function of bulk nickel concentration and as a function of displacement rate, a similar correlation is noted. Those alloys with the greatest segregation (specifically large nickel enrichment compared to chromium depletion), swelling was smaller.

4.2. Influence of material and radiation parameters on swelling

Assuming steady-state point defect concentrations, Mansur derived equations for the void growth rate [31]. The void growth rate for a sink-dominated regime is listed in Eq. (1) while the void growth rate for the recombination-dominated regime is listed in Eq. (2)

$$\frac{\mathrm{d}r_c}{\mathrm{d}t} = \frac{\Omega K_0 Q_i Q_v (Z_i^d Z_v^c - Z_v^d Z_i^c)}{r_c Z_i^d Z_v^d \rho_d (1+Q_i)(1+Q_v)}, \tag{1}$$

$$\frac{\mathrm{d}r_c}{\mathrm{d}t} = \frac{\Omega}{r_c} = \left(\frac{D_i D_v K_0}{Z_i^d Z_v^d R}\right)^{\frac{1}{2}} \frac{Q_i 1/2 Q_v 1/2 (Z_i^d Z_v^c - Z_v^d Z_i^c)}{(1+Q_i)(1+Q_v)}, \tag{2}$$

where

$$Q_{i,v} = \frac{Z_{i,v}^d \rho_d}{4\pi r_c N_c Z_{i,v}^c}$$

and Ω is the atomic volume, r_c the cavity radius, $D_{i,v}$ the interstitial (i) or vacancy (v) diffusion coefficient, K_0 the displacement rate, ρ_d the dislocation density, Z the point defect bias for interstitials (i) or vacancies (v) at dislocations (d) or cavities (c).

As noted in the introduction, as dose rate decreases, swelling rate increases. From Eqs. (1) and (2), it is clear that the production rate of defects K_0 is not the dominant effect since both equations predict swelling to decrease with decreasing dose rate. As noted in the introduction, swelling decreases as bulk nickel increases. The diffusion coefficient of vacancies is known to increase with increasing bulk nickel so vacancy diffusion is not the dominant effect since Eq. (2) predicts swelling to increase with increasing vacancy diffusion. The dislocation density, the point defect bias, or both must be the dominant effect on swelling.

The samples examined in this study had a low dislocation density in the unirradiated state so the recombination-dominated solution is a better description. For very low sink density with $Q_{i,v} \gg 1$ (corresponding to an annealed material with dislocations but no voids), Eq. (2) reduces to:

$$\left.\frac{dr_c}{dt}\right|_{\text{recombination dominated}} \propto \left[\frac{\rho_d}{(4\pi r_c N_c)^2}\right]. \quad (3)$$

Swelling rate will decrease as the void density or size increases. As the cavities nucleate and grow, they compete for a fixed set of point defects produced by the radiation and the growth rate decreases. This effect is shown clearly in Fig. 8, which is adapted from the work of Okita [16]. Below 10 dpa, the ratio in Eq. (3) drops rapidly with dose. Also demonstrated in Okita's work was that at lower doses (less than 22 dpa), the ratio of the density of faulted loops to the total dislocation density increased with increasing dose. Above 22 dpa, no faulted loops were visible, indicating that the faulted loops had unfaulted and joined the network dislocation structure. Following the suggestion of Lee and Mansur that faulted loops had a stronger dislocation bias than network dislocations, Okita's data indicated that at low doses when the differences in swelling are developing, the rate at which faulted loops develop has a strong effect on swelling.

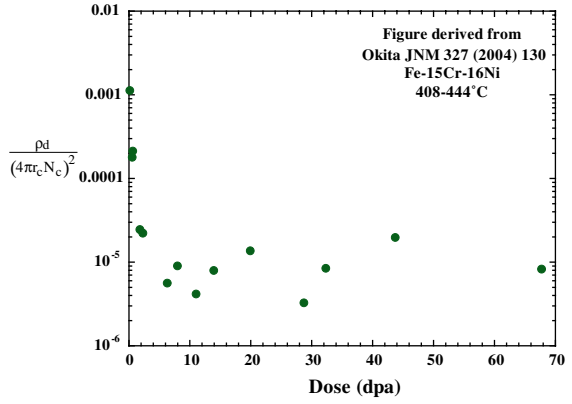

Fig. 8. Changing sink density as a function of dose. The ratio decreases rapidly during the first few dpa when segregation is also developing.

Both this study and the study of Okita clearly showed a correlation between void and dislocation densities at low dose, with the differences in swelling between different alloy compositions correlating with void density and not void size. This study (Fig. 7) also shows that the segregation develops during the same dose range where the dislocation densities change the fastest (shown in Fig. 8). The inference is that changes in segregation at low dose, when the dislocation loop and void densities are developing, may have a significant effect on swelling development.

4.3. Theory of point defect bias and segregation

Segregation can affect void growth through elastic properties. Wolfer et al. showed that a compositional change which increases the shear modulus or lattice parameter locally around a void embryo causes the void to become a preferential sink for vacancies, thus increasing the rate at which embryos mature to voids [19–21]. Wolfer's theory predicts that increasing the shear modulus or lattice parameter locally around a void embryo presents an energy barrier to interstitial motion toward the void. A discrete segregation shell is not required around a void, but the average values in the segregation gradient are adequate to describe the energetics of vacancy motion toward the void.

The segregation shell also affects the void nucleation rate. A segregation shell that increases the shear modulus or lattice parameter locally around a void embryo reduces the nucleation barrier significantly, increasing the probability that the cavity becomes a stable void. In fact, the reduction in the nucleation barrier for a given increase in the shear modulus or lattice parameter is larger in magnitude than the increase in nucleation barrier for a decrease in the shear modulus or lattice parameter of the same magnitude. The predicted effect of changing lattice parameter was more sensitive than the effect of changing shear modulus. An increase of only 0.2% in lattice parameter could significantly increase the void nucleation rate (by roughly six orders of magnitude) while a 1% increase in shear modulus only caused a predicted increase of three orders of magnitude.

For Fe–Cr–Ni alloys with compositions near 304/316 stainless steel, the lattice parameter and shear moduli increase with increasing Cr concentration and decrease with increasing Ni concentration [19]. For such alloys, RIS causes Cr to deplete and Ni to enrich around a void

during irradiation. Figs. 9 and 10 are ternary diagrams for the lattice parameter and shear modulus, respectively, as a function of composition for the Fe–Cr–Ni system. Superimposed on the figure are the shifts in concentration that occur near grain boundaries for an Fe–18Cr–8Ni alloy and an Fe–18Cr–40Ni alloy. For both alloys, the segregation shifts the grain boundary and void shell composition toward regions of smaller lattice parameter and lower shear modulus.

Fig. 11 provides a schematic for a segregation profile at a void surface. To conserve mass, the chromium depletion and nickel enrichment at the void surface must be balanced by chromium enrichment and nickel depletion further into the bulk. Therefore, the void is surrounded by two regions. One region, at the void surface, has a composition that retards void formation and a second region, further into the bulk, which enhances void formation.

4.4. Point defect bias and segregation

The swelling and segregation data in Figs. 2–4 come from three different data sets. The effect of bulk nickel, the effect of the addition of minor elements Mo and P, and the addition of the oversized solute Zr were chosen with the expectation that they would affect swelling and

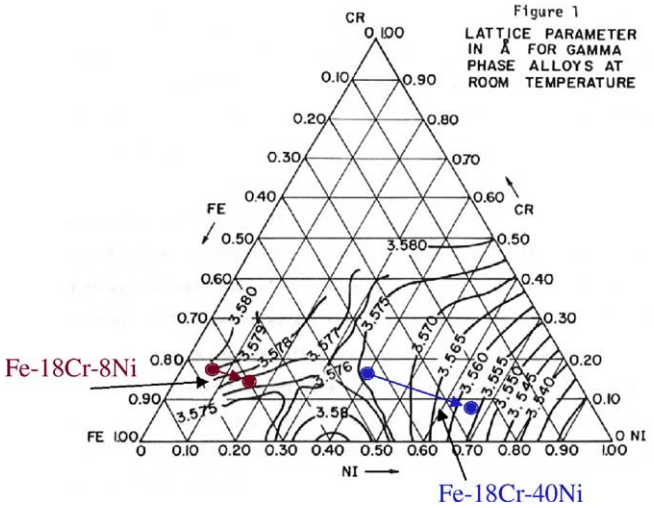

Fig. 9. Lattice parameter as a function of composition in Fe–Cr–Ni alloys (taken from [35]).

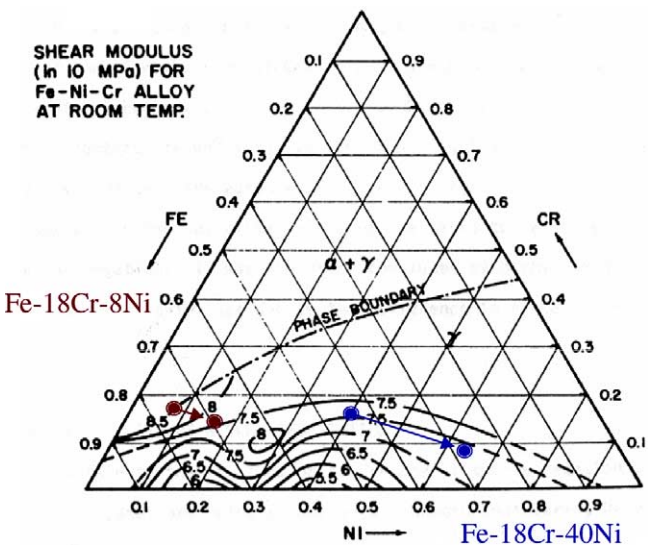

Fig. 10. Shear modulus as a function of composition in Fe–Cr–Ni alloys (taken from [35]).

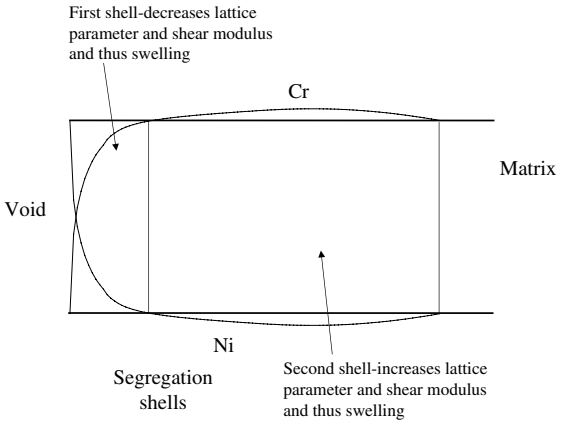

Fig. 11. General schematic of radiation-induced segregation near a void surface.

segregation through different mechanisms. The bulk nickel series was chosen to assess bulk diffusivity effects, the Mo and P to look at chemical ordering effects, and the zirconium series to address the effect of oversized solutes. The three data sets can be examined in combination to examine the interplay between segregation and swelling, in the context of Wolfer's theory.

Fig. 12 plots the swelling as a function of decrease in lattice parameter using all 8 alloys in the data set. The decrease in lattice parameter was extracted from Fig. 9 using the bulk composition to determine the starting lattice parameter. The lattice parameter corresponding to the *measured segregation* was chosen as the final lattice parameter. This choice has two approximations. First, the measured segregation is not equal to the actual segregation. Because of the averaging effect of the TEM probe size (the probe diameter, including beam broadening, is a significant fraction of the segregation profile width and thus averages over a rapidly changing concentration gradient), the measurement underestimates the actual segregation (enrichment or depletion) [36]. Second, as noted above the average concentration in the segregation profile rather than the maximum determines the effect on nucleation and growth. The measured value was chosen as a common reference to compare trends across alloys.

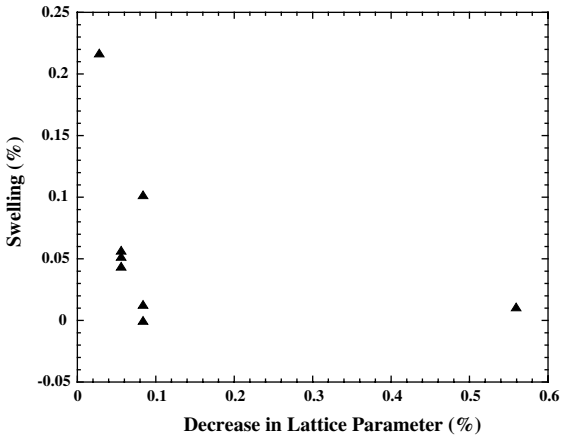

Fig. 12. Decrease in swelling as a function of changing lattice parameter caused by radiation-induced segregation. A decrease in the lattice parameter indicates smaller lattice parameter at the boundary surface.

As can be seen in Fig. 12, those alloys with large decreases in lattice parameter near the boundary resist swelling. This is true regardless of the mechanism that caused the segregation. A similar attempt to correlate swelling with change in shear modulus did not provide a recognizable correlation. As noted above, swelling is expected to be more sensitive to changes in lattice parameter as is apparently seen in this data set.

As explained in the previous section, the second shell, further away from the boundary, is predicted to have a greater effect on swelling because of a greater sensitivity to increases in lattice parameter and shear modulus. Fig. 13 shows a grain boundary segregation profile taken from the Fe–18Cr–40Ni alloy. The 'second shell,' although at times distinguishable, is not always experimentally evident. Although the second shell must exist to conserve mass, in many instances it is below the sensitivity of the STEM-EDS measurements. The small changes in void bias predicted for the large nickel enrichment and chromium depletion near the boundary appear to be more important than the large changes in void bias predicted for the nickel depletion and chromium enrichment in the second shell. This may be due to the 'second shell' being broad with compositions close to the bulk.

A few other comments in the context of this study are important:

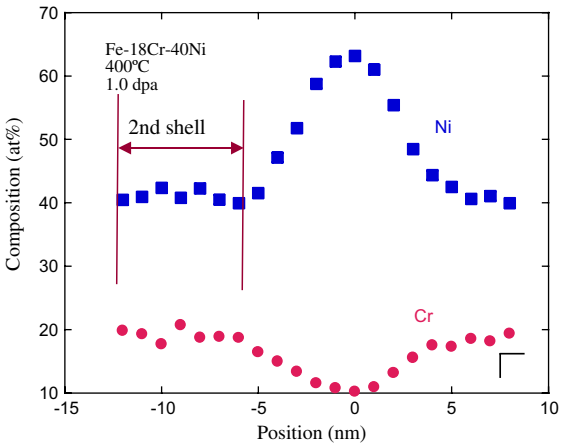

Fig. 13. Typical RIS profile in an irradiated Fe–Cr–Ni alloy.

- Gas atoms are also known to stabilize voids. For these proton-irradiated alloys, the gas loading is not expected to be significant as H is highly soluble so there is no driving force for it to aggregate.
- The effect of minor element segregation on void surface energy has also been noted as a possible contributor to swelling development [19]. This study did not examine the effect of minor elements on surface energy and this effect needs further consideration.
- Previous studies on alloys with higher bulk nickel concentration (those in the INVAR range) indicated a possible spinodal decomposition under radiation [37]. No evidence of a decomposition was noted in this study for these low radiation doses/times.
- The relative bias between voids and loops determines swelling. A more detailed study of segregation at void and loop surfaces as a function of radiation dose would be necessary to fully elucidate the effect of segregation on swelling.
- Future modeling of radiation effects needs to improve the ability to predict microchemical changes and to incorporate these changes into microstructural development.

5. Conclusions

Radiation-induced segregation and swelling were studied in a series of austenitic Fe–Cr–Ni base alloys irradiated with protons at 400 °C to doses of 0.5 and 1.0 dpa. Three alloying effects were examined, the effect of bulk nickel, the effect of the addition of minor elements Mo and P, and the effect of an oversized solute Zr. The addition of nickel in Fe–16–18Cr–*x*Ni caused a significant decrease in swelling and increase in segregation. The addition of Mo+P to Fe–16Cr–13Ni eliminated swelling and reduced segregation. The addition of Zr to Fe–18Cr–9.5Ni decreased swelling and decreased segregation. For alloys where the segregation develops more slowly, the swelling is greatest.

RIS of the major elements correlates with void swelling. Where segregation caused the largest decrease in lattice parameter, the swelling was minimized. The swelling and segregation data were examined in the context of Wolfer's theories on the effect of changes in lattice parameter and shear modulus on point defect bias. The likely mechanism linking segregation to void swelling is through the effect of the local concentration on the lattice parameter, which then change the bias for vacancies diffusing to voids. This correlation held true for all three alloy series, indicating that the correlation between radiation-induced segregation, lattice parameter change, and swelling resistance may be a general effect across austenitic alloys.

Acknowledgement

Thanks to Peter Andresen and the General Electric Corporate Research and Development Laboratory who provided the alloys and to Victor Rotberg and Ovidiu Toader of the Michigan Ion Beam Laboratory for the proton irradiations. Research at the Oak Ridge National Laboratory SHaRE User Facility was sponsored by the Division of Materials Sciences and Engineering, US Department of Energy under contract DE-AC05-00OR22725 with UT-Battelle, LLC. This work was supported by Department of Energy under the award DE-FG07-031D14542 as part of the Nuclear Energy Research Initiative program.

References

[1] C. Cawthorne, J.E. Fulton, Nature 216 (1967) 515.
[2] F.A. Garner, Irradiation performance of cladding and structural steels in liquid metal reactors, in: R.W. Cahn, P. Haasen, E.J. Kramer (Eds.), Materials Science and Technology, A Comprehensive Treatment, Nuclear Materials, vol. 10A, VCH, Weinheim, 1994.
[3] W.G. Johnston, J.H. Rosolowski, A.M. Turkalo, T. Lauritzen, J. Nucl. Mater. 54 (1974) 24.
[4] Busby, J.T., Allen, T.R., Gan, J., Kenik, E.A., Was, G.S., in: Proceedings of Eighth International Symposium on Environmental Degradation of Materials in Nuclear Power Systems-Water Reactors, August 10–14, 1997, Amelia Island Fl.
[5] J.F. Bates, W.G. Johnston, in: Proceedings of International Conference on Radiation Effects in Breeder Reactor Structural Materials, The Metallurgical Society of AIME, Scottsdale, New York, 1977, p. 625.
[6] T. Kato, H. Takahashi, M. Izmiya, Mater. Trans. JIM 32 (10) (1991) 921.
[7] T. Kato, H. Takahashi, M. Izmiya, J. Nucl. Mater. 189 (1992) 167.
[8] G.M. Bond, B.H. Sencer, F.A. Garner, M.L. Hamilton, T.R. Allen, D.L. Porter, in: Proceedings of 9th International Conference on Environmental Degradation of Materials in Nuclear Power Systems, Water Reactors, 1999, p. 1045.
[9] F.A. Garner, D.J. Edwards, S.M. Bruemmer, S.I. Porollo, Yu.V. Konobeev, V.S. Neustroev, V.K. Shamardin, A.V. Kozlov, in: Proceedings, Fontevraud 5, Contribution of Materials Investigation to the Resolution of Problems Encountered in Pressurized Water Reactors, 23–27 September, 2002, paper #22, on CD format, no page numbers.
[10] V.S. Neustroev, V.K. Shamardin, Z.E. Ostrovsky, A.M. Pecherin, F.A. Garner, Effects of Radiation on Materials: 19th International Symposium, in: M.L. Hamilton, A.S. Kumar, S.T. Rosinski, M.L. Grossbeck (Eds.), ASTM STP, 1366, American Society for Testing and Materials, 2000, p. 792.
[11] F.A. Garner, S.I. Porollo, A.N. Vorobjev, Yu.V. Konobeev, A.M. Dvoriashin, V.M. Krigan, N.I. Budylkin, E.G. Mironova, International Symposium on Contribution of Materials Investigation to the Resolution of Problems

Encountered in Pressurized Water Reactors, 14–18 September 1998, Fontevraud, France, p. 249.
[12] S.I. Porollo, A.N. Vorobjev, Yu.V. Konobeev, A.M. Dvoriashin, F.A. Garner, International Symposium on Contribution of Materials Investigation to the Resolution of Problems Encountered in Pressurized Water Reactors, 14–18 September 1998, Fontevraud, France, p. 271.
[13] V.S. Neustroev, V.K. Shamardin, Z.E. Ostrovsky, A.M. Pecherin, F.A. Garner, International Symposium on Contribution of Materials Investigation to the Resolution of Problems Encountered in Pressurized Water Reactors, 14–18 September 1998, Fontevraud, France, p. 261.
[14] F.A. Garner, N.I. Budylkin, Yu.V. Konobeev, S.I. Porollo, V.S. Neustroev, V.K. Shamardin, A.V. Kozlov, in: 11th International Conference on Environmental Degradation of Materials in Nuclear Power Systems – Water Reactors, 2003, issued on CD format, p. 647.
[15] E.H. Lee, L.K. Mansur, Phil. Mag. 52 (4) (1985) 493.
[16] T. Okita, W.G. Wolfer, J. Nucl. Mater. 327 (2004) 130.
[17] P.R. Okamoto, L.E. Rehn, J. Nucl. Mater. 83 (1979) 2.
[18] A.D. Marwick, J. Phys. F.: Metal Phys. 8 (1978) 1849.
[19] A. Si-Ahmed, W.G. Wolfer, Effects of Radiation on Materials: Eleventh Conference, in: H.R. Brager, J.S. Perrin (Eds.), ASTM STP, 782, American Society for Testing and Materials, 1982, p. 1008.
[20] W.G. Wolfer, L.K. Mansur, J. Nucl. Mater. 91 (1980) 265.
[21] J.J. Sniegowski, W.G. Wolfer, in: Proceedings of Topical Conference on Ferritic Alloys for Use in Nuclear Energy Technologies, Snowbird, Utah, 19–23 June 1983.
[22] D.L. Damcott, J.M. Cookson, V. Rotberg, G.S. Was, Nucl. Inst. Meth. Phys. Res. B 99 (1995) 780.
[23] C. Brown, Developments in Electron Microscopy and Analysis, in: J.V. Venables (Ed.), Academic Press, London, 1976.
[25] E.A. Kenik, J. Nucl. Mater. 216 (1994) 157.
[26] T.R. Allen, J.T. Busby, G.S. Was, E.A. Kenik, J. Nucl. Mater. 255 (1998) 44.
[27] D.L. Damcott, T.R. Allen, G.S. Was, J. Nucl. Mater. 225 (1995) 97.
[28] G.S. Was, T. Allen, J. Nucl. Mater. 205 (1993) 332.
[29] T.R. Allen, J.I. Cole, E.A. Kenik, Effects of Radiation on Materials: 20th International Symposium, in: S.T. Rosinski, M.L. Grossbeck, T.R. Allen, A.S. Kumar (Eds.), ASTM STP, 1405, American Society for Testing and Materials, West Conshohocken, PA, 2002, p. 427.
[30] T.R. Allen, G.S. Was, Acta Met. 46 (1998) 3679.
[31] L.K. Mansur, J. Nucl. Mater. 216 (1994) 97.
[32] R. Guillou, M. Guttmann, Ph. Dumoulin, Metal Sci. (February) (1981) 63.
[33] D.L. Damcott, J.M. Cookson, R.D. Carter Jr., J.R. Martin, M. Atzmon, G.S. Was, Rad. Eff. Def. Solids 118 (1991) 383.
[34] T.R. Allen, J.T. Busby, J. Gan, E.A. Kenik, G.S. Was, Effects of Radiation on Materials: 19th International Symposium, in: M.L. Hamilton, A.S. Kumar, S.T. Rosinski, M.L. Grossbeck (Eds.), ASTM STP, 1366, American Society for Testing and Materials, West Conshohocken, PA, 2000, p. 739.
[35] W.G. Wolfer, F.A. Garner, L.E. Thomas, Effects of Radiation on Materials: Eleventh Conference, in: H.R. Brager, J.S. Perrin (Eds.), ASTM STP, 782, American Society for Testing and Materials, 1982, p. 1023.
[36] R.D. Carter, D.L. Damcott, M. Atzmon, G.S. Was, E.A. Kenik, J. Nucl. Mater. 205 (1993) 361.
[37] F.A. Garner, J.M. McCarthy, K.C. Russell, J.J. Hoyt, J. Nucl. Mater. 205 (1993) 411.